The free energy $\mathcal{F}_N$ can be obtained by measuring the partition coefficient (i.e., the ratio of concentration inside the pore to the concentration outside) for a pore exchanging chains with a bulk solution:[7]

$$\frac{C_{pore}}{C_{bulk}} \sim \exp\left(-\frac{\mathcal{F}_N}{kT}\right) \quad (23)$$

We have thus a process to separate long versus small chains from a blend of chemically identical chains.

(2) For D smaller than $l_3 = aP$, the threshold length N_C becomes sensitive to the confinement.

In the case of a slit, N_C is given by $N_C = N_{C2} \equiv PD/a$. For $N < N_{C2}$, the chain is ideal. For $N > N_{C2}$, the chain can be pictured as a sequence of ideal pancakes (of size $l_2 = aN_{C2}^{1/2}$) that exclude each other: $R = (N/N_{C2})^{\nu_2} l_2$. By analogy with the previous case, we postulate that the free energy of confinement is proportional to the number N/N_{C2} of units[12]

$$\mathcal{F}_N = \frac{N}{N_{C2}}kT = \frac{N}{P(D/a)}kT \quad (D/a < P) \quad (24)$$

For a true two-dimensional problem, we obtain $\mathcal{F}_N = (N/P)kT$.

In the case of a capillary, $N_C = N_{C1} \equiv P^{2/3}(D/a)^{4/3}$ if $P^{1/4} < D/a < P$. For $N < N_{C1}$, the chain is ideal. For $N > N_{C1}$, the chain is a sequence of ideal sausages (of size $l_1 = aN_{C1}^{1/2}$) that exclude each other: $R = (N/N_{C1})l_1$. The free energy of confinement should be given by[13]

$$\mathcal{F}_N = \frac{N}{N_{C1}}kT = \frac{N}{P^{2/3}(D/a)^{4/3}} \quad (P^{1/4} < D/a < P) \quad (25)$$

For a very small capillary, all the chains are spatially segregated. The N chain fills a portion of the tube of length $L = Na^3/D^2$. The confinement energy can be expected to be given by $\mathcal{F}_N = (N/P)kT$, which does coincide with (25) for $D = aP^{1/4}$.

B. Since the role of the P chains is to reduce the monomer–monomer interactions of the N chain, our theory should apply equally to dilute polymer solutions with small excluded-volume parameters ($0 \ll v \leq a^3$).

Acknowledgment. We have benefited from stimulating discussions with P.-G. de Gennes and H. Hervet. We thank the referees for their useful comments and suggestions.

References and Notes

(1) Flory, P. J. *J. Chem. Phys.* **1949**, *17*, 303.
(2) Edwards, S. F. *Proc. Phys. Soc.* **1966**, *88*, 265.
(3) Flory, P. J. *Principles of Polymer Chemistry*; Cornell University Press: Ithaca, NY, 1971; Chapter XII. Huggins, M. *J. Am. Chem. Soc.* **1942**, *64*, 1712.
(4) Daoud, M.; de Gennes, P.-G. *J. Phys. Fr.* **1977** *38*, 85. See also: Turban, J. *J. Phys. Fr.* **1984**, *45*, 347.
(5) Brochard, F.; de Gennes, P.-G. *J. Phys. Lett. Fr.* **1979**, *40*, 399.
(6) Raphael, E.; Brochard-Wyart, F. *CRAS* **1989**, *309II*, 963.
(7) Colton, C. K.; Satterfield, C. M.; Lai, C. J. *AIChE.* **1975**, *21*, 289.
(8) Guillot, G.; Leger, L.; Rondelez, F. *Macromolecules* **1985**, *18*, 2531.
(9) Satterfield, C.; Katzer, J. R. *Adv. Chem. Ser.* **1971**, *102*, 19.
(10) de Gennes, P.-G. *Scaling Concepts in Polymer Physics*; Cornell University Press: Ithaca, NY, 1985.
(11) de Gennes, P.-G. *Macromolecules* **1980**, *13*, 1069.
(12) One cannot simply justify eq 24 by the lose of entropy due to the confinement since the structures at small scales of the free chain (spheres of size l_3) and of the confined chain (pancakes of size l_2) are different. By definition, the repulsive energy per unit (l_3 or l_2) is given by kT. The increase in the number of subunits from N_{c3} to N_{c2} leads thus to a contribution to $\mathcal{F}_N$: $((N/N_{c2}) - (N/N_{c3}))kT \sim (N/N_{c2})kT$, which is of the same oder as the entropic term.
(13) One can use the same argument as in ref 12 provided that one replaces N_{C2} by N_{C1}.

Configurational Characteristics and Scaling Behavior of Starburst Molecules: A Computational Study

Robert L. Lescanec and M. Muthukumar*

Polymer Science and Engineering Department, University of Massachusetts, Amherst, Massachusetts 01003. *Received July 17, 1989; Revised Manuscript Received November 2, 1989*

ABSTRACT: The growth of starburst molecules having trifunctional branch points and flexible spacers of P (= 1, 3, 5, 7, 9, and 11) steps are studied by a computer simulation. A self-avoiding walk algorithm is employed to kinetically grow the molecules. The center-to-branch-end distance is found to scale with the radius-of-gyration of the molecule throughout growth. Intramolecular density profiles indicate that the ends of the branches traverse the entire molecule and are not confined to its surface. This branch growth behavior indicates highly folded branches throughout all stages of growth. In general, kinetically grown models of starburst molecules behave as modified Cayley trees. The radius of gyration, R_g, of the molecule is found to scale with the molecular weight M and the spacer length P according to $R_g \sim M^{\nu}P^{\beta}$. The exponents β and ν change throughout growth with $\nu = 0.22 \pm 0.02$ and $\beta = 0.50 \pm 0.02$ in the high molecular weight scaling region.

Introduction

The scaling behavior of "starburst" growth was originally considered by Zimm and Stockmayer in their study of branched polymers.[1] The resulting structural form has fallen under the nomenclature of a Cayley tree or Bethe lattice in much of the physics literature, especially in percolation theory.[2,3] Generalizations of the Zimm–Stock-

0024-9297/90/2223-2280$02.50/0

mayer theory have been performed to account for excluded volume and its effects.[4-6] The study of the statistical properties of starlike polymers has attracted recent interest due to the controlled synthesis of successive generations of starburst polymers by Tomalia and coworkers.[7,8]

Since their first synthesis, efforts have been made to explain the growth mechanisms and the observed physical behavior of these polymers. Maciejewski, discussing their "host–guest" character, placed starburst molecules in the structural realm of "cast shells".[9] Then a calculation, based on this notion, using a modified version of Edwards' self-consistent fields[10] was performed by de Gennes and Hervet.[11] Their calculation predicted the molecular dimensions, intramolecular density profiles, limits of growth, and the scaling behavior of starburst polymers. The tacit assumption present in their development is that the branches become elongated as the molecule grows with the branch ends lying on the surface of the molecule throughout all stages of growth. Growth termination would then result from space-filling considerations on the surface. Recently, Naylor and Goddard[12] performed a molecular dynamics simulation of starburst molecules, yielding molecular dimensions and intramolecular structural detail. Their starburst molecules were generated by using energy minimization techniques, accounting for bonded as well as nonbonded interaction potentials.

In this paper we present a kinetic growth model of starburst molecules. The molecules considered in this simulation have trifunctional branch points with flexible spacers between pairs of branch points. The simulation algorithm grows all branches of the same generation simultaneously. The functionality of the branch points and the spacer lengths studied are selected to closely match ideal synthetic conditions.[7]

In this study spacer length is the primary parameter of the simulation. For each spacer length the intramolecular density profile, radius of gyration of the molecule, and the center-to-end distance of the branches, hence known as the "starburst radius", are calculated as each generation is grown. A major objective is to determine the location of the ends of the branches at each stage of growth. Knowledge of the molecular structure is necessary to further understand the mechanisms of synthesis and explain the observed physical behavior of these molecules.

Model and Simulation Technique

The scope of this study is to simulate the growth of starburst molecules having trifunctional branch points, with the number of steps between these branch points remaining constant throughout the growth of a single starburst molecule. Note that although the number of steps between connected branch points remains constant, the distance between them varies statistically. The algorithm is an off-lattice simulation in three dimensions. The excluded volume effect is considered by allowing the molecule to grow in a self-avoiding walk fashion. No dynamics are employed in this model; therefore no molecular relaxation takes place during growth or after growth termination. A single starburst molecule is grown, statistics are compiled, and then the procedure is repeated. Thus, this model is kinetic rather than thermodynamic in character.

The growth of a starburst molecule begins by placing a bead at the center of a defined coordinate system. This bead is the beginning of the first generation of the molecule and will be a trifunctional branch point or junction, that is, having three connected neighbors. One step of length l is taken from the center of this bead, and if there is no bead overlap, the center of the first bead of the first spacer is placed. This happens two additional times to ensure that this first junction is trifunctional. The algorithm then returns to the first spacer and tries to place the second bead by taking one step (of length l) from the first bead. If this is successful, the algorithm will proceed to the second spacer and then to the third. This happens P times in total, with P being the number of steps in a spacer. The last three beads placed will complete the first generation and each will be trifunctional. (In general the last $3(2^{N-1})$ beads will complete the Nth generation.) The algorithm will take two steps from each of these beads in a similar fashion as described above. The molecules are grown in this way to ensure that all of the branches grow uniformly, as they would in an ideal synthesis. Growth of the molecule is terminated when the algorithm is unable to place a bead, due to excluded volume arising from local bead crowding, after a sufficient number of attempts. The molecule is then truncated to the last completed generation and constitutes a statistical sample.

For each sample, the bead density distribution, the mean-squared radius of gyration and the mean-squared starburst radius are calculated for each completed generation. The bead density distribution, expressed as a volume fraction, is found by dividing space into spherical shells centered around the coordinate system employed (the configurational center of the molecule) and counting the number of beads in a given shell. The volume fraction, ϕ, at a given radial distance, r (from the configurational center), is the total volume of spherical beads in the shell divided by the volume of the shell. The mean-squared radius of gyration is calculated in the manner outlined by Zimm and Stockmayer.[1] The mean-squared starburst radius is defined to be the average-squared distance from the center of the coordinate system to the trifunctional beads at the end of a generation.

Here spacer steps of P = 1 (Cayley tree), 3, 5, 7, 9, and 11 are the cases of the simulation. The bead diameter is 1 (arbitrary units) and the step length l is 1.2. These values are selected to prevent bond crossing which cannot exist in a physical system. The algorithm makes 5000 attempts when placing a bead before terminating growth. For each spacer length 5000 statistical samples are evaluated.

Results and Discussion

Parts a through d of Figure 1 show the spatial structure of a typical starburst molecule having a spacer length, P = 5, through four generations of growth. The branch ends at the completion of each generation are indicated by dots. It is apparent that the ends are not confined to the surface of the molecule. Significant chain folding occurs which becomes quite evident as the molecule grows. This is in contrast to the general assumption that the chain ends migrate toward the surface of the molecule with starburst growth terminating due to space filling on the surface.[8,11]

Figure 2 shows the growth distribution for 5000 samples at P = 5. Note that over 60% of the samples are between six and seven generations with the average being 6.3 ± 0.6 generations for this spacer length. Generally, as spacer length increases, the growth distribution skews toward higher average generations. The values for these average generations (±10%) versus spacer length are plotted in Figure 3 along with the limiting predictions of de

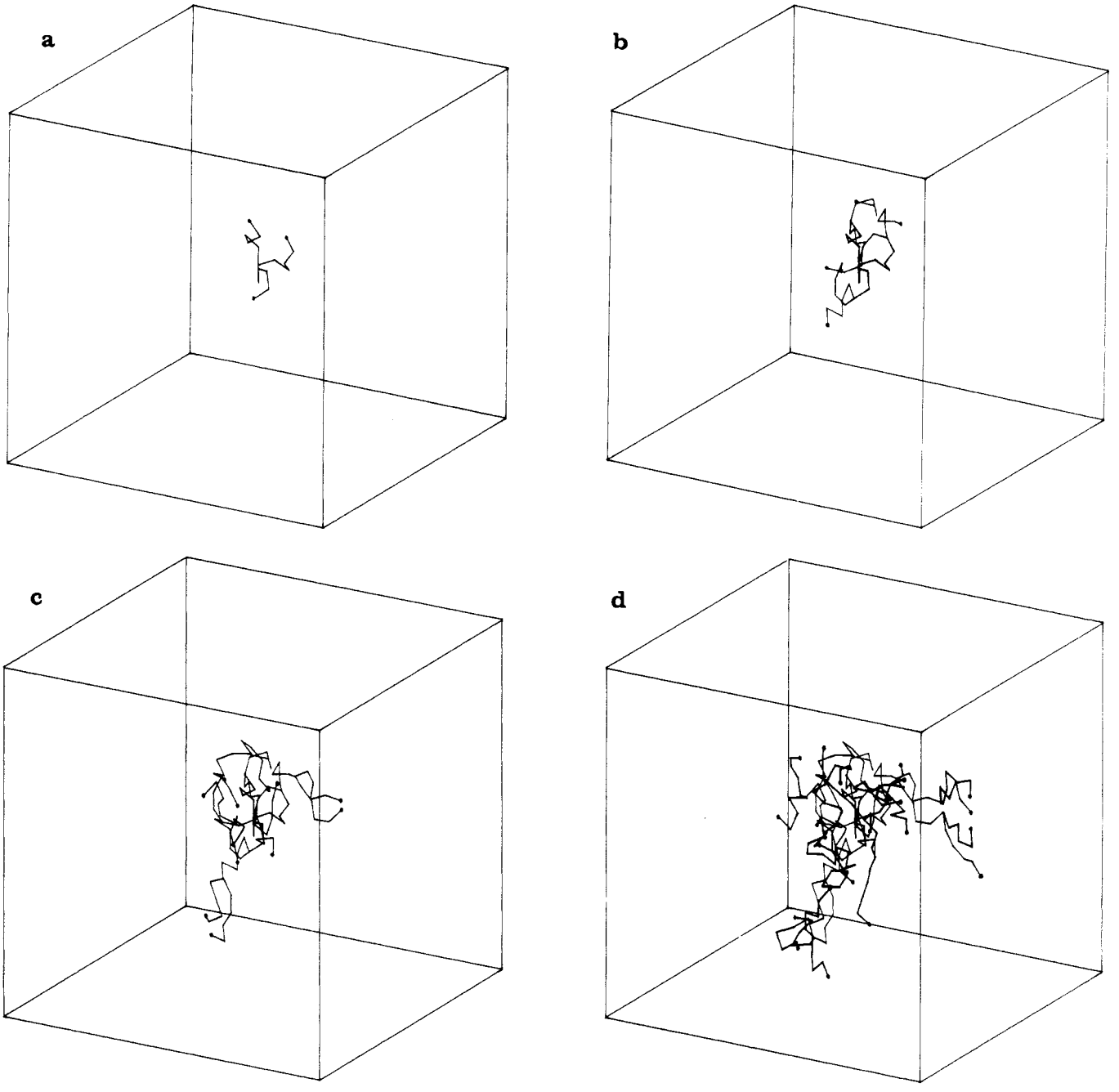

Figure 1. Typical starburst configuration for (a) one, (b) two, (c) three, and (d) four generations with spacer length, $P = 5$.

Gennes and Hervet.[11] Note that the simulation data show asymptotic behavior at high values of P, while the theoretical prediction is logarithmic in P. As mentioned, the theoretical prediction (±0.02) is for the limiting generation number, that is, the maximum number of generations a sample of spacer length P can attain. The simulation data for $P = 3$, 5, 7, 9, and 11 lie below the theoretical maximum. However for $P = 1$, the Cayley tree case, the simulation average lies above the theoretical maximum for generations grown. These discrepancies can be attributed to the fact that the theoretical prediction is valid for large values of P (long spacers) while the simulation used short spacers.

Figure 4 shows intramolecular bead density (expressed as a volume fraction) profiles for $P = 5$ through 7 generations of starburst growth. The profiles are typical for all values of P in this study. This plot shows that the starburst molecule has highest densities near its center with the density monotonically decreasing outward from the configurational center (not to be confused with the center of mass) of the molecule. The density profiles show consistent shape, with the density at a given radial distance increasing with molecular growth. Note that at $r = 1$ this increase is quite small and is not commensurate with the increase shown at all other radial distances. With the stated bead diameter and bond length used in the simulation it is easily shown that only the center of one bead can fit in the shell at $r = 1$, with that bead being the initial trifunctional junction of the molecule. The slight spread in this density ($\phi = 0.125$) is well within the error of ±10% for volume fractions greater than 0.01. The density at the average starburst radius (the average location of branch ends) at each generation, shown by asterisks, is included on these profiles. Significant molecular density exists radially beyond the average starburst radius at all stages of growth. From this it is clear that the ends of the molecule do not lie on its surface.

Since the density of the molecule increases uniformly throughout the molecule as shown (except at $r = 1$), the growing end must interpenetrate the molecule at all stages

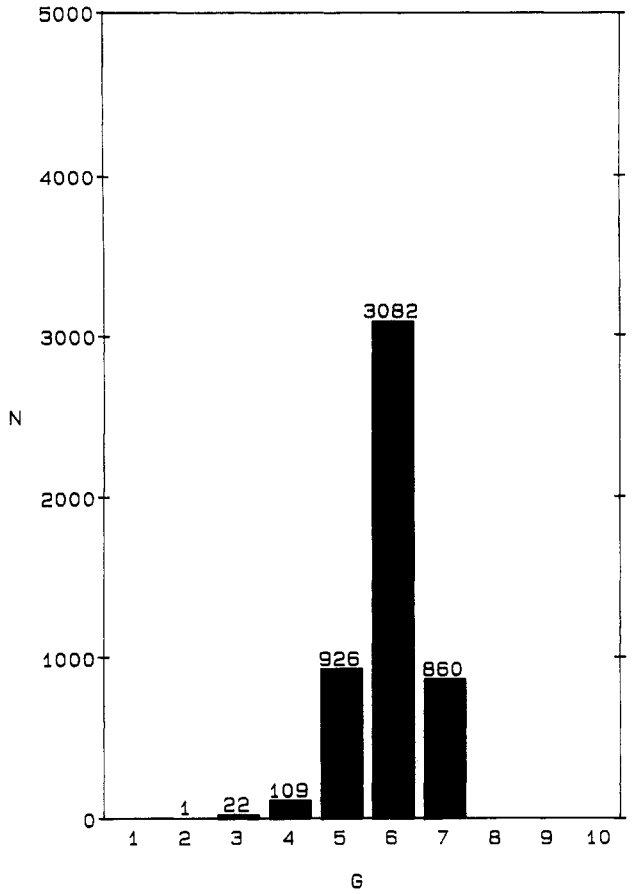

Figure 2. Starburst growth distribution for 5000 samples with $P = 5$. The number of molecules (N) is plotted as a function of highest generation (G) attained in growth.

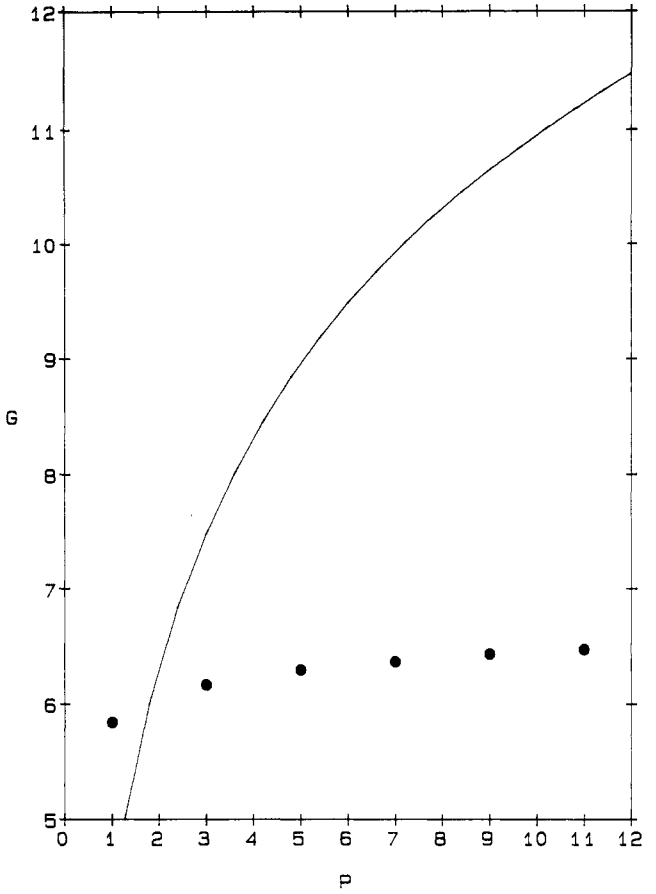

Figure 3. Comparison of experimental averages (●) with the limiting predictions of de Gennes and Hervet (—) for starburst growth (in generations) versus spacer length, P.

of growth. If the growing ends were always confined to the surface, the density at the inner shells would quickly plateau during the early stages of growth and the entire profile would be exponential in r.[11] It is clear that the molecule does not grow radially from its configurational center.

Parts a through d of Figure 5 show density profiles for each spacer length, as indicated by the key, at one, three, four, and seven generations, respectively. The starburst radius for each spacer length is also included and is again indicated by an asterisk. These density profiles are calculated in the same manner as those in Figure 4 and show a similar error of ±10% at volume fractions greater than 0.01. The density profiles in parts a through d of Figure 5 have the same shape as those in Figure 4 for the reasons mentioned. The trends in the profiles as a function of spacer length are the primary focus of these figures.

Figure 5a shows that by the end of the first generation, the density at a given radial distance from the configurational center of the molecule increases with increasing spacer length. This results from increased chain folding that naturally occurs with increasing spacer length. Since the molecule has only three branches at the end of this generation, density increases in this "core" region ($r < 10$) as these branches become highly folded. At the end of the second generation, this behavior continues; however, the core region is extended radially.

By the end of the third generation, Figure 5b, an inversion in the profiles is seen. At radial distances less than $r = 3$ the density decreases with increasing spacer length at a given r, the opposite of what is seen for generations one and two. However when $r > 3$, the same behavior is seen for the first two generations as previously described. Parts c and d of Figure 5, for four and seven generations, respectively, show that the transition in the density profile becomes more pronounced as the molecule grows. Note also that the transition region moves radially outward from the configurational center as the molecule grows.

The behavior of the density profiles from generations three through seven results from the buildup of the core region seen in generations one and two. As spacer length increases, the core region becomes more dense and consequently the growing branches have difficulty penetrating this region during the later stages of growth. Conversely, molecules whose branches are short (small P) can more easily interpenetrate the core region and contribute density to this region more effectively than molecules with long spacers which preferentially grow outward from the center, thus avoiding core interpenetration. This results in increasing density with increasing spacer length outside the transition region.

With R and R_g denoting the average starburst radius and the average radius of gyration respectively, Figure 6 is a double logarithmic plot of R/R_g versus molecular weight. The molecular weight, M, is the number of beads in the molecule. Note that $M = N + 1$ where N is the number of bonds (self-avoiding steps) in the molecule. Each datum for each spacer length is taken as the completion of a generation. The purpose is to obtain the scaling relationship of R and R_g with the error in each of these quantities of ±10%. From this plot the following scaling law, which is valid for all M, is obtained:

$$R/R_g \sim M^{-0.03\pm0.02} \quad (1)$$

From this it is apparent that $R \sim R_g$ within error. Therefore, from this point onward only R_g will be considered in further discussion.

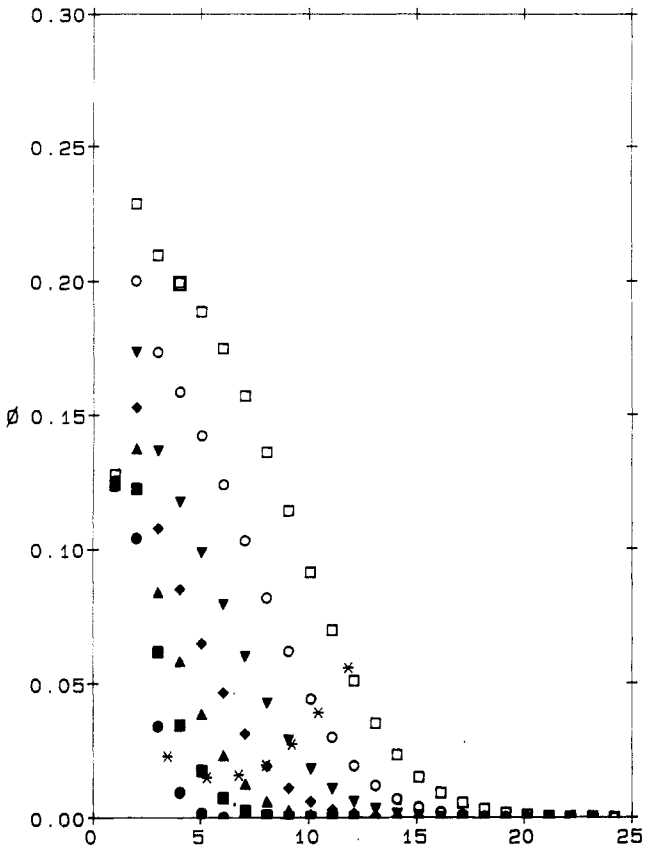

Figure 4. Density profiles as a function of generation for $P = 5$. Here, ϕ is the bead volume fraction at distance r from the configurational center. Growth is shown through one (●), two (■), three (▲), four (♦), five (▼), six (○), and seven (□) generations. Note that the asterisks (*) indicate the location of the branch ends in the density profile at each generation of growth.

Figure 7 attempts to scale the values for R_g (or R) found in the simulation according to the relation given by de Gennes and Hervet. They state that the length scale is $P^{0.4}$ for these measured quantities. The spacers carry a statistical weighting when compared to the junctions in their development. Figure 7 is a double logarithmic plot of $R_g/P^{0.4}$ versus M/M_s with $M_s/M_j = 1$. Here M_s is the molecular weight counting only spacer beads and M_j is the molecular weight based on counting only trifunctional junction beads. The data show similar behavior when $M_s/M_j \rightarrow \infty$ (the limiting case of massless junction beads) is considered. From this plot the following scaling law is obtained, for high molecular weights:

$$R_g/P^{0.4} \sim (M/M_s)^{0.22\pm0.02} \quad (2)$$

The scaling relationship is in agreement with the theoretical prediction with respect to molecular weight M; however, no universal collapse of the curves is seen. This is an indication that the length scale of $P^{0.4}$ used in these plots is inappropriate in scaling the data for the low values of P studied here. Note however that the curves show a trend to collapse as P is increased which indicates that $P^{0.4}$ may be the proper length scale at large P.

It is critical that the proper length scale for the system be determined in order to establish scaling laws and determine the physical behavior of the system. Figure 8 is a double logarithmic plot of R versus M_b, the branch molecular weight. As before, data are taken at the end of each complete generation through generation seven (generation six for $P = 1$). M_b at the end of a given generation is simply the size of the molecule (in generations) multiplied by P. Here branches are considered as single chains, and effective end-to-end distances are measured. From the figure it is seen that an extensive linear region exists which exhibits the scaling relation:

$$R \sim M_b^{0.57\pm0.05} \quad (3)$$

Since $M_b \sim P$, R (and consequently R_g) $\sim P^{0.5-0.6}$. Due to the limited accuracy of the simulation, a broader range is given to the value of the exponent in P. This range also suggests physically limiting cases of branch behavior ranging from random-walk statistics to self-avoiding walk statistics. Note that the branches do not behave as rodlike or stiff molecules ($R \sim M_b$), as they would if the spacers were elongated. In the latter stages of growth of the molecule (greater than five generations) positive deviations from linearity are seen in the data. The deviations are most severe for very short spacers. This indicates that as the branches re-enter the dense region of the molecule branch, stretching is seen from an effective core potential. Since the core region is built up more slowly as spacer length increases, the stretching is delayed to successively later stages of growth as spacer length increases.

On the basis of this branch behavior, attempts were made to scale the data in Figure 7 using a length scale of $P^{0.5}$ and $P^{0.6}$. Both of these length scales were explored to determine the range of growth statistics seen in the development of a starburst molecule. No universal collapse of the data was seen at $M_s/M_j = 1$ or at $M_s/M_j \rightarrow \infty$. However one limit exists that has not been considered thus far when scaling the molecular weight of the system. This is the limit of $M_s/M_j = 0$ where the spacers have no effective molecular weight and only the branch points have mass. The spacers only provide a length scale for the walk of the branch points.

Figure 9 shows the scaling behavior as this limit is explored by using a length scale of $P^{0.5}$. A length scale of $P^{0.5}$ collapses the data at high molecular weights, while a length scale of $P^{0.6}$ is seen to collapse the data at low molecular weights. This indicates that the excluded volume effect seen early in growth becomes screened during the later stages of growth where overall molecular density increases. From Figure 9 the following scaling law is seen at high molecular weights:

$$R_g/P^{0.5} \sim M^{0.22\pm0.02} \quad (4)$$

Again note that M is the molecular weight based only on the branch points. According to this scaling law the molecule exhibits a fractal dimension, d_f of ~ 4 at large M. This behavior results from the highly branched structure of the molecule. Zimm and Stockmayer[1] show the following scaling behavior for a Cayley tree:

$$R_g \sim M^{0.25} \quad (5)$$

Figure 10 shows this for the Cayley tree at large M. Molecular weight here is the total molecular weight of the molecule counting both branch and spacer beads equally. In this figure no length scale is used and therefore the curves will not collapse. Only during the later stages of growth (generations five through seven) does the molecule exhibit Cayley tree scaling behavior when $P = 1$. During the early stages of growth the molecule has a fractal dimension of ~ 2. As growth continues, the fractal dimension smoothly increases with molecular weight, ultimately exhibiting Cayley tree behavior.

As spacer length is increased, the fractal dimension of the molecule is seen to slightly increase throughout all stages of growth. Limiting values of ν ($1/d_f$) are shown in Figure 10 for $P = 11$. It is clear then that spacer length

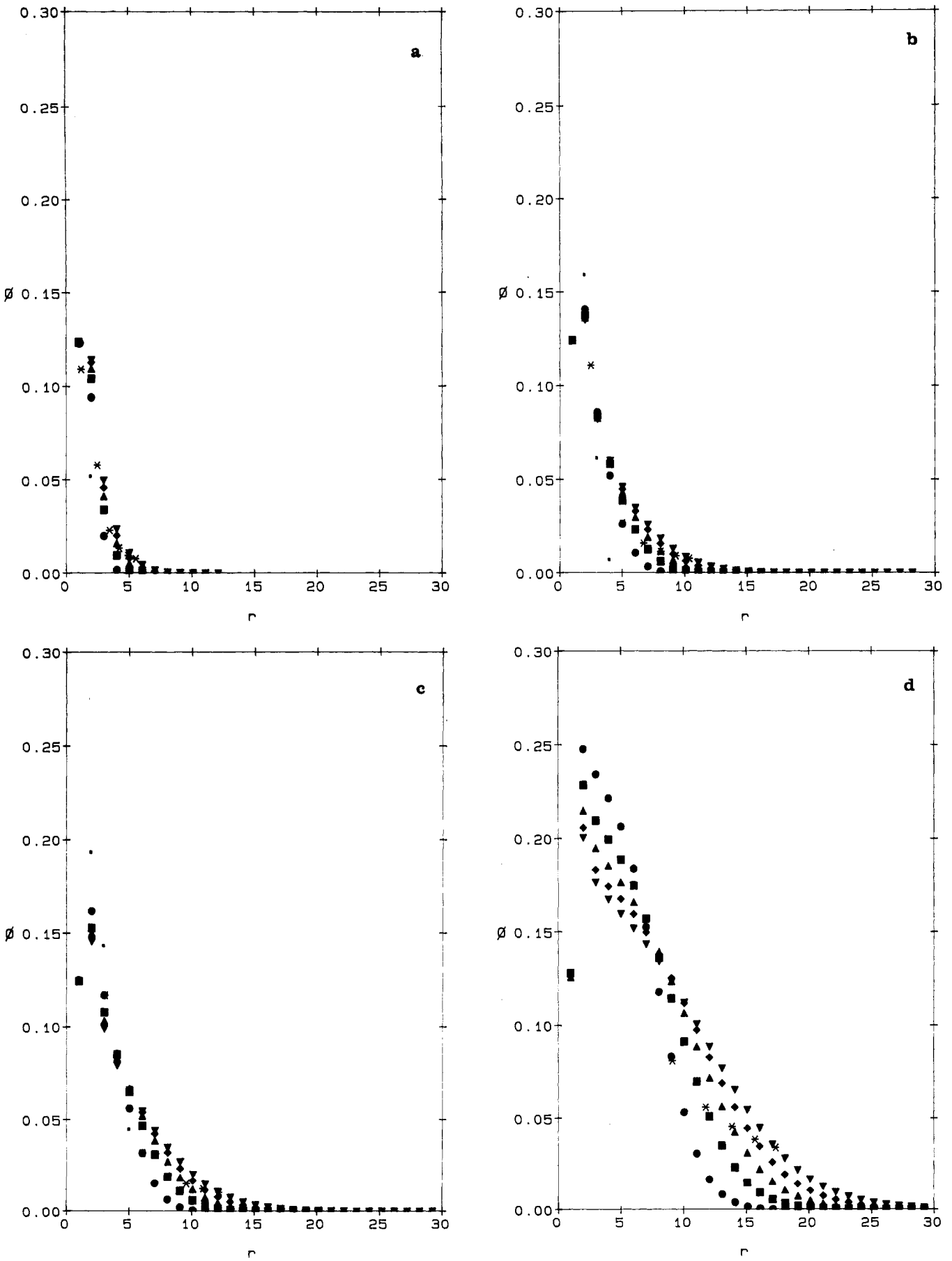

Figure 5. Density profiles as a function of spacer length at (a) one, (b) three, (c) four, and (d) seven generations of growth. ϕ is the bead volume fraction at distance r from the configurational center. Spacer lengths of 1 (·), 3 (●), 5 (■), 7 (▲), 9 (♦), and 11 (▼) are shown. The asterisks (*) indicate the location of the branch ends in the density profile for each spacer length.

affects the fractal dimension of the molecule throughout growth. The consideration of spacers in this study shows that starburst molecules develop into "modified" Cayley trees.

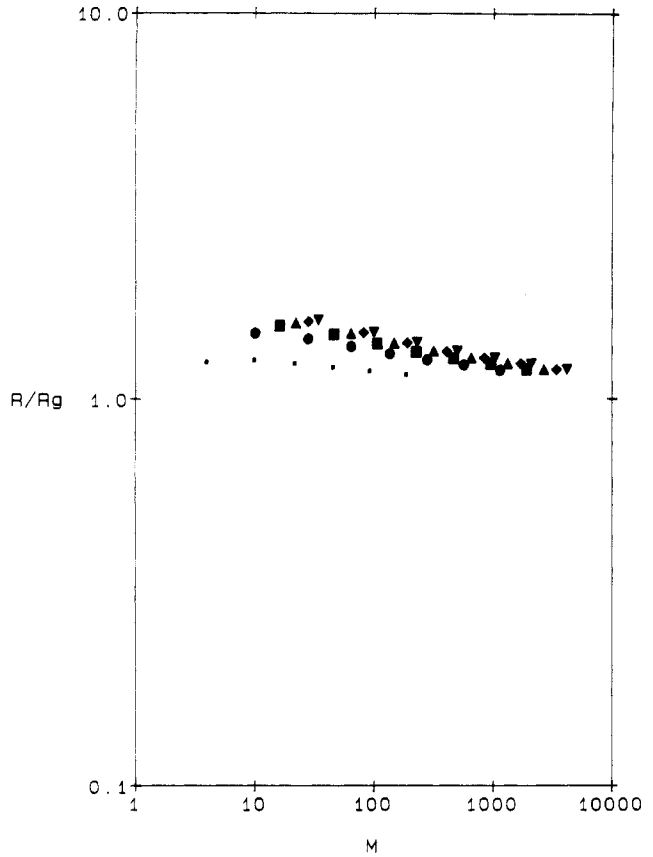

Figure 6. R/R_g versus M as a function of spacer length, P. The spacer lengths used are indicated in Figure 5.

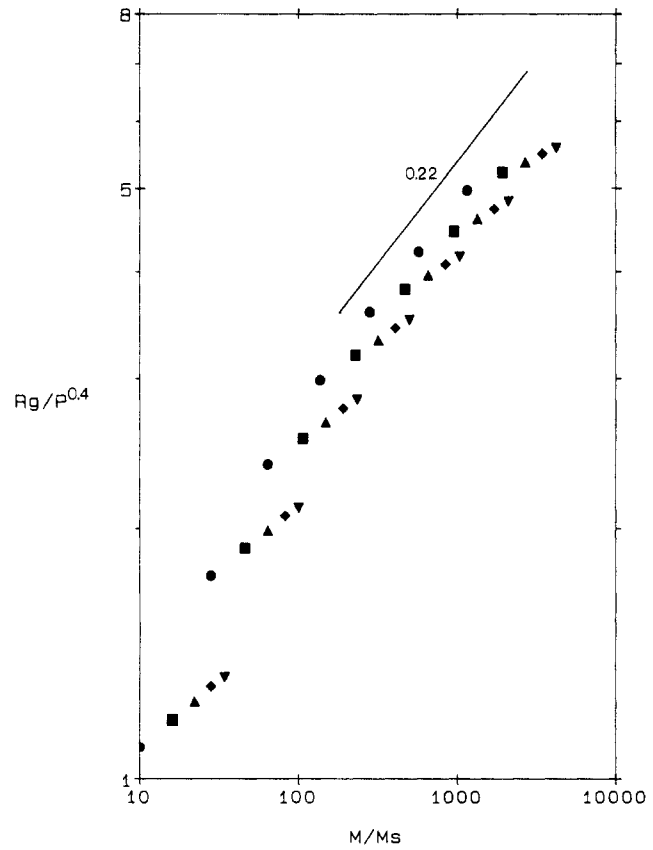

Figure 7. $R_g/P^{0.4}$ versus M/M_s as a function of spacer length, P, for $M_s/M_j = 1$. All spacer lengths indicated in Figure 5 are shown except for $P = 1$.

During the initial stages of growth, Cayley tree scaling is not seen because of the small degree of branching.

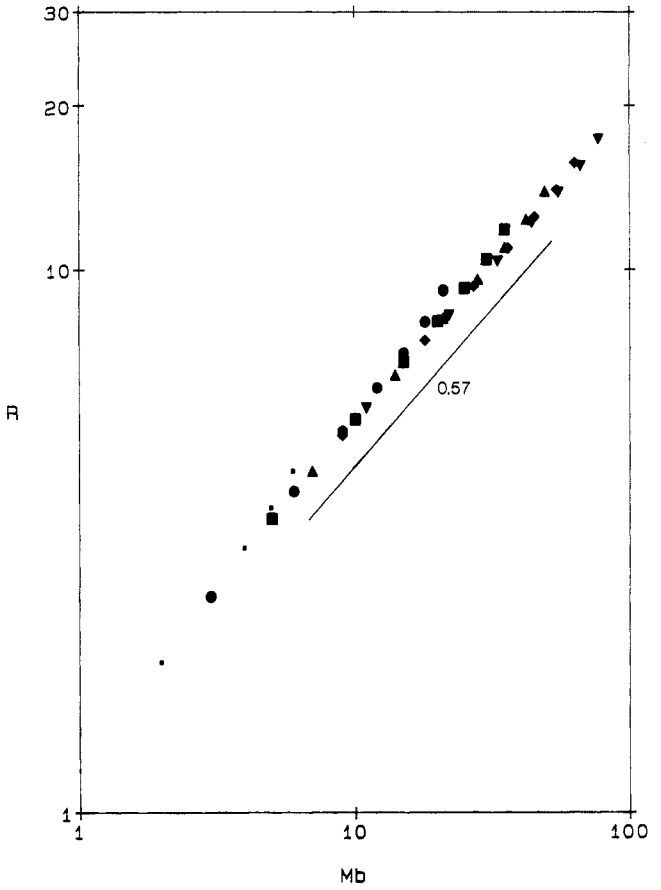

Figure 8. R versus the branch molecular weight, M_b, as a function of spacer length. See Figure 5 for a key to the spacer lengths shown.

The fractal dimension during the first few generations is ~2. Daoud and Cotton predict a fractal dimension of 2 for star polymers with short arms in dilute solution.[6] At the end of one generation each starburst molecule is a three-arm star. Thus, the scaling behavior during the early stages of growth is expected to approach that seen by Daoud and Cotton. Therefore, initially these starburst polymers behave as ordinary stars in terms of their scaling behavior. However, later in growth, the branching nature of the molecule becomes more developed and the statistics reflect a "modified" Cayley tree scaling behavior.

An implication of the behavior of the fractal dimension of the molecule at different generations is its interesting intrinsic viscosity behavior. Figure 11 is constructed using the limiting data from Figure 10 and the well-known scaling relationship for intrinsic viscosity:[13]

$$[\eta] \sim M^{3\nu-1} \tag{6}$$

This figure shows a maximum in the double logarithmic plot of intrinsic viscosity versus molecular weight. This maximum will be shifted toward higher molecular weights as spacer length is increased. This implies that as the polymer grows its hydrodynamic radius initially increases. However, at a certain molecular weight, determined by spacer length, a transition occurs with the relative increase in hydrodynamic radius decreasing with further growth. Thus, $[\eta] \sim M^{0.5}$ in the early stage and $[\eta] \sim M^{-0.4}$ in the late stage of growth.

An implication of the observed chain folding behavior is its effect on NMR experiments. Meltzer and Tirrell[14] used ^{13}C NMR to determine the correlation times for the carbon atoms located within the spacer backbone and the branch ends. They found that carbons along the spac-

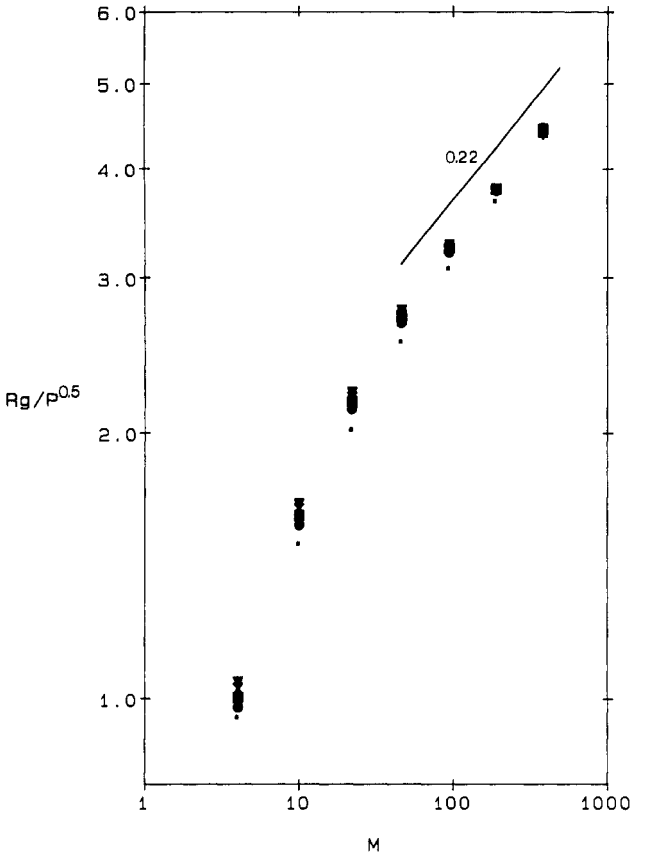

Figure 9. $R_g/P^{0.5}$ versus M as a function of spacer length with $M_s/M_j = 0$. See Figure 5 for a key to the spacer lengths shown.

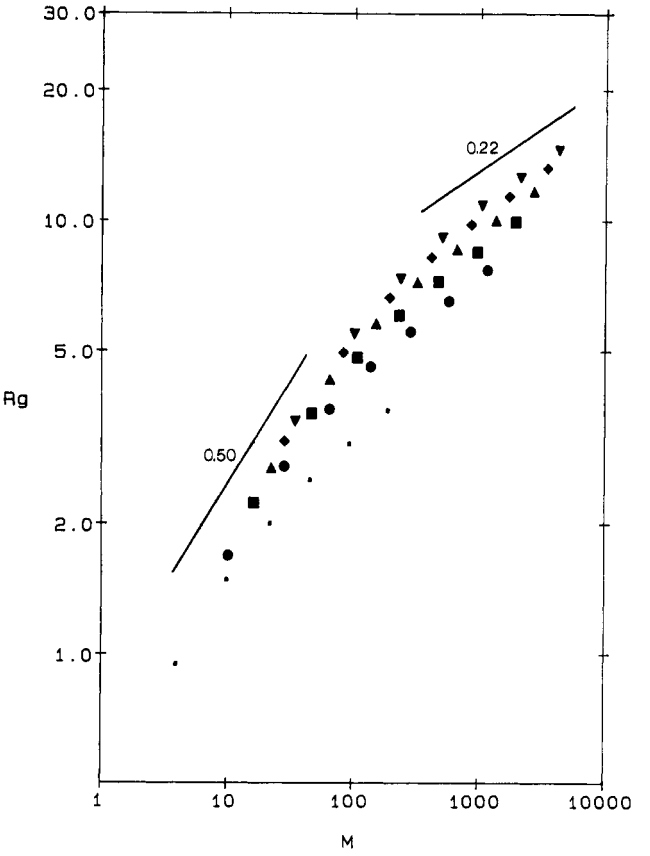

Figure 10. R_g versus M as a function of spacer length. Note that $M_s/M_j = 1$ and the spacer lengths used are indicated in Figure 5.

ers were less mobile than those at the branch ends at all molecular weights. This is expected since the carbon atoms located at the branch ends are less sterically hindered than those in the backbone of the spacer. Furthermore this is consistent with the present simulation results, indicating that the branch ends do not pack on the surface of the molecule, which would restrict their mobility. They also noted that the carbon atoms located within the spacers as well as those at the branch ends at a given generation became less mobile as the molecule grew. This may result from branch folding which causes the branch ends to interfere with the spacer mobility and vice versa.

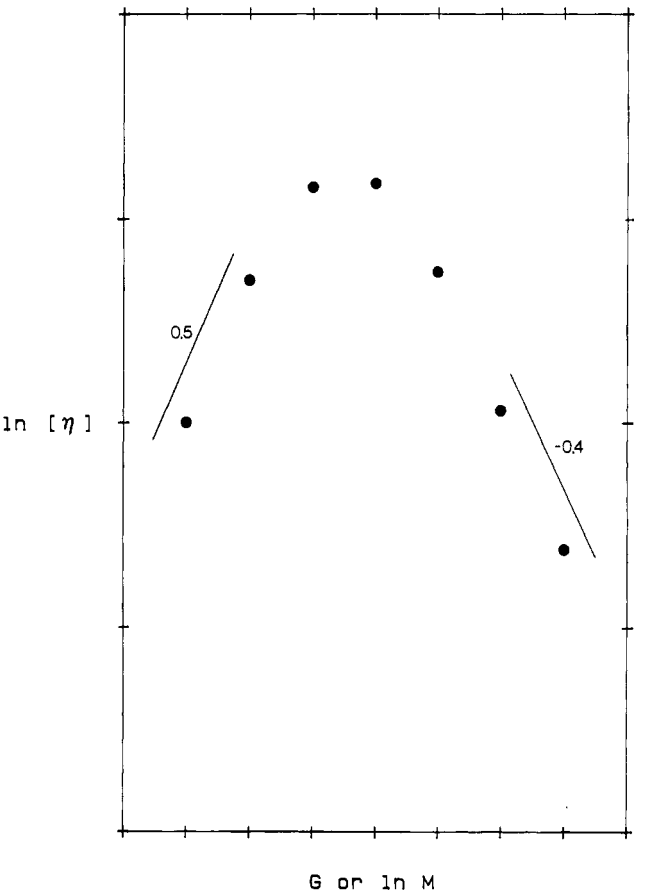

Figure 11. Calculated plot of ln [η] verus generation, G or ln M. Note that $M_s/M_j = 1$.

Conclusions

The starburst molecules have been simulated by a kinetic growth method, and the results show significant differences from those previously predicted.[9,11] The most significant of these differences is the fact that the ends of the branches at a given generation are not on the surface but may be buried within the molecule. This fact results in a density distribution that strongly differs from the prediction of the self-consistent field calculation of de Gennes and Hervet. The statistics presented and the physical properties derived show a strong, nonuniversal dependence on spacer length. In the high molecular weight regime, $R_g \sim M^{\nu}P^{\beta}$ with $\nu = 0.22$ and $\beta = 0.5$.

It must be duly noted that the simulation presented deals with short spacers as opposed to those in the self-consistent field theory. However, the spacers modeled in the present simulation are of comparable length to those studied experimentally.[7,8] The folding behavior of the branches modifies the classical Cayley tree structure that dominates the statistical analysis during the latter stages of growth. Evidence of this folding is seen in ^{13}C NMR determination of the correlation times of spacer-backbone and branch-end carbon atoms. During growth, the transition in the molecule's configurational behavior from "starlike" to "modified Cayley tree" greatly influ-

ences its hydrodynamic behavior which would be seen in intrinsic viscosity measurements.

The growth of starburst molecules in the present study is using the algorithm of kinetic self-avoiding walk.[15] It is of interest to know whether such an algorithm leads to a faithful description of equilibrium structures of starburst molecules studied experimentally.[7,8] Since it has been shown that a kinetic self-avoiding walk for a linear flexible chain lies in the same universality class[16,17] as the conventional self-avoiding walk in equilibrium, we expect that the conclusions drawn in our study are applicable to the starburst molecules at equilibrium also.

Finally, in an effort to establish the equilivalence between the kinetically grown starburst molecules and equilibrium structures, preliminary development of an algorithm that relaxes the kinetically grown starburst molecules was undertaken. However, initial results indicate that excessive computational time is required to relax these structures due to the large number of particles present. This precludes future work in this area at this time.

Acknowledgment. This work is supported by NSF Grant DMR-8420962. We are grateful to A. D. Meltzer, Prof. D. A. Tirrell, and Prof. D. A. Hoagland for several conversations regarding the problem addressed here.

References and Notes

(1) Zimm, B. H.; Stockmayer, W. H. *J. Chem. Phys.* **1949,** *17,* 1301.
(2) Stauffer, D. *Introduction to Percolation Theory*; Taylor and Francis: London, 1985.
(3) Stauffer, D.; Coniglio, A.; Adam, M. *Adv. Polym. Sci.* **1982,** *44,* 103.
(4) Lubensky, T. C.; Isaacson, J. *Phys. Rev.* **1979,** *A20,* 2130.
(5) Muthukumar, M. *J. Chem. Phys.* **1985,** *83,* 3161.
(6) Daoud, M.; Cotton, J. P. *J. Phys. (Les Ulis, Fr.)* **1982,** *43,* 531.
(7) Tomalia, D. A., et al. *Macromolecules* **1986,** *19,* 2466.
(8) Tomalia, D. A.; Berry, V.; Hall, M.; Hedstrand, D. M. *Macromolecules* **1987,** *20,* 1167.
(9) Maciejewski, M. *J. Macromol. Sci., Chem.* **1982,** *A17* (4), 689.
(10) Edwards, S. F. *Proc. Phys. Soc., London* **1965,** *93,* 605.
(11) de Gennes, P.-G.; Hervet, H. *J. Phys., Lett.* **1983,** *44,* L351.
(12) Naylor, A. M.; Goddard, W. A. *Polym. Prepr. (Am. Chem. Soc., Div. Polym. Chem.)* **1988,** *29* (1), 215.
(13) de Gennes, P.-G. *Scaling Concepts in Polymer Physics*; Cornell University: Ithaca, 1979.
(14) Meltzer, A. D.; Tirrell, D. A. Unpublished results.
(15) Majid, I.; Jan, N.; Coniglio, A.; Stanley, H. E. *Phys. Rev. Lett.* **1984,** *52* (15), 1257.
(16) Peliti, L. *J. Phys., Lett.* **1984,** *45,* L925.
(17) Kremer, K.; Lyklema, J. W. *Phys. Rev. Lett.* **1985,** *55* (19), 2091.

Weak Polyelectrolytes between Two Surfaces: Adsorption and Stabilization

Marcel R. Böhmer,* Olaf A. Evers, and Jan M. H. M. Scheutjens

Laboratory for Physical and Colloid Chemistry, Wageningen Agricultural University, Dreijenplein 6, 6703 HB Wageningen, The Netherlands. *Received June 26, 1989; Revised Manuscript Received October 18, 1989*

ABSTRACT: A theory has been developed for adsorption from solution of weak flexible polyelectrolytes in a gap between two surfaces. The theory is an extension of the self-consistent-field theory of Scheutjens and Fleer for adsorption of uncharged homopolymers. The finite volume of solvent molecules, polyelectrolyte segments, and ions is taken into account using a multi-Stern-layer model. The dielectric constant and the degree of dissociation of polyelectrolyte segments are allowed to vary with position between the surfaces. Results for the potential decay in the electrical double layer are shown. The effect of salt concentration and pH on the adsorption of polyelectrolyte is also studied. With increasing salt concentration more polyelectrolyte chains adsorb and the adsorbed layer becomes more extended. A maximum in the amount of adsorbed polyelectrolyte is found as a function of the counterion concentration. For a polyacid this maximum is at a pH which is 1–1.5 units below pK. Like for uncharged polymers, the interaction between the two surfaces is mainly determined by the adsorbed amount. A low adsorbed amount leads to a deep minimum in the free energy of interaction, due to bridging, at a small separation. A high adsorbed amount leads to a shallow minimum at large surface separation. At smaller separation strong repulsion dominates, due to steric hindrance. If the polyelectrolyte is completely charged, electrostatic repulsion dominates the interaction curve at large separation. As the adsorption depends strongly on salt concentration and pH, the interaction between two surfaces in the presence of an adsorbing polyelectrolyte can in principle be controlled. If the polyelectrolyte does not adsorb, a depletion layer near the surface develops, which becomes thinner with decreasing salt concentration. At small surface separation, when polyelectrolyte has been depleted from between the surfaces, a Donnan equilibrium is established. This results in a stronger attraction than in a situation where electrostatic charges are absent.

Introduction

A few years ago, a theory for the adsorption of linear flexible polyelectrolytes was presented by Van der Schee and Lyklema.[1] These authors showed that electrostatic interactions can be incorporated in lattice-based models for polymer adsorption, such as Roe's model[2] and the self-consistent-field (SCF) theory of Scheutjens and Fleer.[3,4] In these theories the shape of the concentration profile near a surface is not predetermined but is

* To whom all correspondence should be addressed.

0024-9297/90/2223-2288$02.50/0